

# Organic-Inorganic Molecular Nano-Sensors: A Bis-Dansylated Tweezer-Like Fluoroionophore Integrating a Polyoxometalate Core

Mauro Carraro,<sup>\*[a]</sup> Gloria Modugno,<sup>[a]</sup> Giulia Fiorani,<sup>[a]</sup> Chiara Maccato,<sup>[a]</sup>  
Andrea Sartorel,<sup>[a]</sup> and Marcella Bonchio<sup>\*[a]</sup>

*Dedicated to Professor Gianfranco Scorrano on the occasion of his retirement*

**Keywords:** Hybrid materials / Nanostructures / Sensors / Trace analysis / Copper / Polyoxometalates

Functionalization of the bis-lacunary Keggin polyoxotungstate  $[\gamma\text{-SiW}_{10}\text{O}_{36}]^{8-}$  has been achieved with a two-step synthesis, by the covalent attachment of a 3-aminopropylsilane spacer and further linkage of the dansyl (5-dimethylamino-1-naphthalenesulfonyl-) residue. The resulting bis-decorated molecular hybrid  $[\{[(\text{CH}_3)_2\text{N}]\text{C}_{10}\text{H}_6\text{SO}_2\text{NH}(\text{CH}_2)_3\text{Si}\}_2\text{O}(\gamma\text{-SiW}_{10}\text{O}_{36})]^{4-}$  has been isolated and characterized in solution and in the solid state by FTIR, multinuclear NMR, ESI-MS, UV/Vis, luminescence spectroscopy, dynamic light scattering (DLS), and Scanning Electron Microscopy (SEM). The inorganic polyoxometalate provides a molecular nano-surface where the dansyl fluorophores are anchored with a tweezer-type arrangement. The merging of the organic and inorganic domains of the bis-dansylated complex dictates its fluorescence features, which are observed in the range 375–600 nm,

its amphiphilic properties, and the multi-site recognition/signaling of cationic analytes due to the complementary effect of the tungsten oxide polyanionic surface.

Indeed, the interplay of the appended sulfonamide moieties and of the molecular metal oxide fosters an enhanced selectivity for  $\text{Cu}^{2+}$  and  $\text{Pb}^{2+}$  ion sensing, even in the presence of potentially interfering cations such as  $\text{Co}^{2+}$ . These latter are preferentially captured by the inorganic platform. By virtue of its hybrid nature, the title fluoroionophore evolves to supramolecular architectures and extended systems in mixed organic solvent/aqueous environment, yielding spherical vesicles and macroporous thin films. Flat polymeric membranes incorporating the hybrid fluorophore can also be obtained, suggesting the generation of heterogeneous sensing devices that integrate both filtration and separation functionalities.

## Introduction

Polyoxometalates (POMs) are nano-dimensional molecular, multi-metal oxides, which have found applications in catalysis, materials science, and nano-medicine.<sup>[1–4]</sup> Tailored control of their properties is readily achieved by tuning the elemental composition, structure, and charge density of the inorganic scaffold.<sup>[1]</sup> Moreover, the introduction of surface-bound organic arms is a valuable tool for shaping the stereoelectronic features of the resulting hybrid complexes, as well as their solubility, redox behavior, spectroscopic response, and hydrolytic stability in various media.<sup>[5,6]</sup> Indeed, the merging of organic and inorganic domains on POM nano-scaffolds is a developing field of investigation focusing on the design of new functional molecules and materials.<sup>[7,8]</sup> POM-appended organic/organometallic moieties are instru-

mental for advanced catalytic applications<sup>[9]</sup> and can direct the supramolecular organization of the hybrid molecules evolving to extended nanostructures.<sup>[10]</sup> The interplay of organic chromophores and POMs by covalent linkage and ionic assembly has been recently proposed to promote charge separation states, being instrumental for solar energy conversion and storage, as well as for the development of molecular capacitors and photosensitized catalytic processes.<sup>[11,12]</sup> Considering the interdisciplinary frontier of inorganic nano-clusters in medicinal chemistry, the design and synthesis of POM hybrids is appealing because it should be possible to enhance the bio-availability, modify delivery strategies, and to introduce tailored recognition/signaling sites.<sup>[13]</sup> In this latter field, luminescent POMs have been proposed for bio-imaging/sensors and could eventually couple the diagnostic potential with innovative therapy protocols.<sup>[14]</sup> To this end, the use of totally inorganic lanthanide-substituted POMs suffers from extensive luminescence quenching in aqueous environment coupled to a narrow-range pH stability.<sup>[15]</sup> A promising alternative stems from decoration of the POM scaffold with resident lumino-phores, whereby covalent bonds guarantee long-term performance under physiological conditions.

[a] Istituto per la Tecnologia delle Membrane del CNR, Sezione di Padova and Department of Chemical Sciences, University of Padova,  
1, via Marzolo, 35131 Padova, Italy  
E-mail: mauro.carraro@unipd.it  
marcella.bonchio@unipd.it

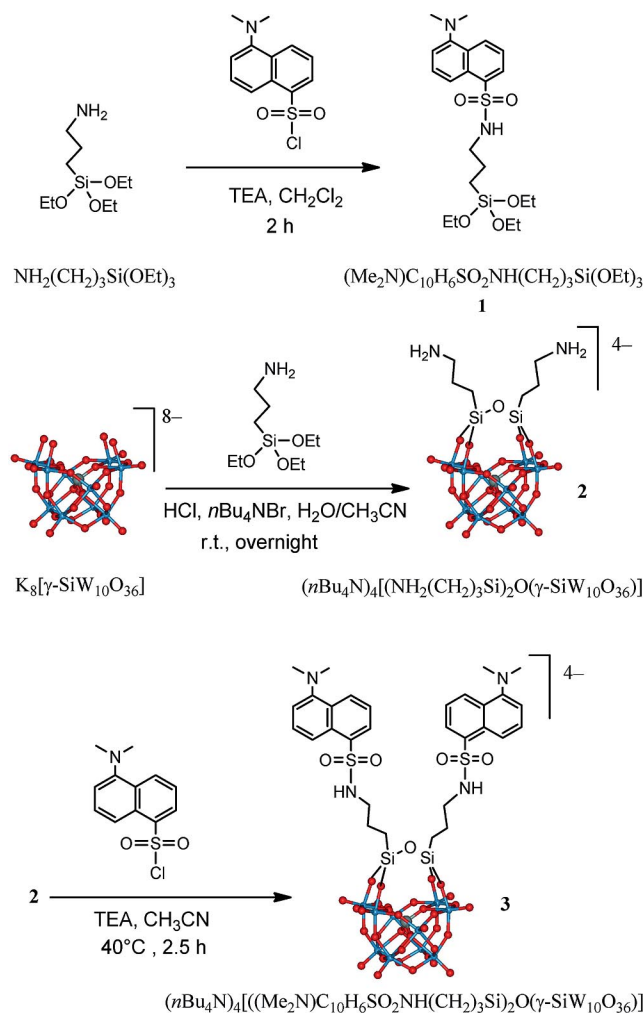
Supporting information for this article is available on the WWW under <http://dx.doi.org/10.1002/ejoc.201101122>.

We report herein the synthesis of a luminescent POM hybrid, obtained by selective functionalization of the lacunary Keggin-type polyoxotungstate  $[\gamma\text{-SiW}_{10}\text{O}_{36}]^{8-}$  with 5-dimethylamino-1-naphthalenesulfonyl (generally indicated as dansyl) chromophore. The dansyl label carries some key optical properties, such as: (i) intense fluorescence in the visible region; (ii) relatively long emission wavelength; (iii) a high Stokes shift behavior preventing self quenching; (iii) solvatochromism, by effect of a twisted intramolecular charge-transfer (TICT) excited state, and (iv) selective excitation/absorption response of the protonated state, leading to antenna-effects in polydansylated arrays.<sup>[16,17]</sup> These unique features have been successfully exploited for the molecular design of fluorescent chemosensors in which the dansyl chromophore is used in combination with receptor domains, including multi-dentate ligands,<sup>[18]</sup> supramolecular hosts such as calix[4]arenes,<sup>[19]</sup> cyclodextrins,<sup>[20]</sup> crown ethers,<sup>[21]</sup> and also nano-silica surfaces.<sup>[22]</sup> Depending on the dansyl environment, selective fluoroionophores have been obtained with interesting sensitivity towards ions such as  $\text{Pb}^{2+}$ ,<sup>[23]</sup>  $\text{Hg}^{2+}$ ,<sup>[18,24]</sup> and  $\text{Cu}^{2+}$ .<sup>[19,25]</sup> In particular, a strong signal amplification results from multi-cooperative fluorescence quenching involving a dansylated surface-array attached to tailored nanosensors.<sup>[17,26]</sup> Our innovative approach targets the molecular scaffold of inorganic polyoxometalates with the final aim to (i) shape a tweezer-like arrangement of the luminophore residues at the optical signaling site; (ii) provide a polyanionic environment for complementary charge recognition events; (iii) evaluate the amphiphilic properties of the luminescent hybrid and its supramolecular/thin film self-organization for sensitivity enhancement and membrane processes. A comparison with the monomeric 3-(dansylamido)propyl(triethoxy)silane (**1**) has also been included to evaluate the impact of the POM-assisted signaling phenomena.

## Results and Discussion

Covalent derivatization of POM surfaces occurs smoothly according to well-established synthetic strategies, in analogy to those applied for the functionalization of extended metal oxides. Herein, selective dansylation of the vacant polyoxotungstate  $[\gamma\text{-SiW}_{10}\text{O}_{36}]^{8-}$  has been achieved after introduction of an aminopropyl trialkoxysilane spacer. The reaction entails a double functionalization of the POM precursor at the tetra-oxygenated nucleophilic site, which occurs readily in acetonitrile under phase-transfer conditions, by addition of  $n\text{Bu}_4\text{NBr}$ .<sup>[27,6a]</sup>

The resulting intermediate  $[\{\text{NH}_2(\text{CH}_2)_3\text{Si}\}_2\text{O}(\gamma\text{-SiW}_{10}\text{O}_{36})]^{4-}$  (**2**),<sup>[6a,11a]</sup> which was characterized by heteronuclear NMR and FTIR spectra (see the Supporting Information), reacts in a post-functionalization step with dansyl chloride (3.5 equiv.) in the presence of triethylamine (TEA, 3.5 equiv.), in acetonitrile at 50 °C for 2.5 h (Scheme 1). The final product  $(n\text{Bu}_4\text{N})_4[\{(\text{CH}_3)_2\text{N}\}_2\text{C}_{10}\text{H}_6\text{SO}_2\text{NH}(\text{CH}_2)_3\text{Si}\}_2\text{O}(\gamma\text{-SiW}_{10}\text{O}_{36})]$  (**3**) was isolated in 69% yield, after precipitation with water and purification by extensive washing/extraction cycles with diethyl ether and acetone.



Scheme 1. Synthetic route to **3**.

The FTIR spectrum of **3** (see the Supporting Information, Figure S8), features diagnostic bands between 982 and 737  $\text{cm}^{-1}$  (W–O bonds) and weak absorption at 1101 and 1045  $\text{cm}^{-1}$  (Si–O), furthermore, comparison with the spectra of  $[\gamma\text{-SiW}_{10}\text{O}_{36}]^{8-}$  and **2** confirms the integrity of the hybrid POM network upon dansylation. The new absorption bands observed at 1318 and 1143  $\text{cm}^{-1}$  result from the sulfonamidic substituents. The ESI-MS spectrum of **3**, recorded in the negative mode, shows a dominant cluster centered at  $m/z = 773.9$  that can be ascribed to  $[\{(\text{CH}_3)_2\text{N}\}_2\text{C}_{10}\text{H}_6\text{SO}_2\text{NH}(\text{CH}_2)_3\text{Si}\}_2\text{O}(\gamma\text{-SiW}_{10}\text{O}_{36})]^{4-}$ , confirming the expected functionalization pattern, and the introduction of two dansyl units through a bis-sulfonamide linkage involving both amino pendants on the POM surface (Figure S9).

The novel hybrid POM **3** exhibits  $^{29}\text{Si}$  and  $^{183}\text{W}$  NMR spectral patterns confirming, respectively, the bis-organosilane anchoring ( $^{29}\text{Si}$  NMR:  $\delta = -62.5$  ppm, 2Si), in addition to the central tetrahedral  $\text{SiO}_4$  group ( $^{29}\text{Si}$  NMR:  $\delta = -88.4$  ppm, 1Si; Figure S10), and the overall  $C_{2v}$  symmetry of the POM structure with a 2:1:2 intensity ratio of the three expected  $^{183}\text{W}$  NMR signals ( $^{183}\text{W}$  NMR:  $\delta = -107.9, -136.2, -142.1$ ; Figure S11).<sup>[21,22]</sup>

The  $^1\text{H}$  and  $^{13}\text{C}$  NMR spectra were also consistent with the expected covalent conjugate and, in particular, the signals of the aromatic carbons of **3** are sensibly deshielded (115–153 ppm), with respect to the dansyl chloride precursor (115–135 ppm), the  $\alpha$  methylene protons resonate at  $\delta = 2.84$  ppm ( $\Delta\delta = -0.7$  ppm with respect to dansyl-free **2**), and the amidic ( $\text{SO}_2\text{NH}$ ) proton resonates at  $\delta = 5.95$  ppm, which is a chemical shift close to that obtained for the reference derivative **1** in the same solvent ( $\delta = 5.82$  ppm).<sup>[28]</sup>

The UV/Vis spectrum of **3** ( $>200$  nm) displays a shoulder at 218 and a maximum at 250 nm, together with a broad absorbance tail extending up to 450 nm. This spectral behavior is the result of the POM oxygen-to-tungsten charge-transfer bands overlapping with the typical absorption features of the fluorophore moiety, as can be seen from the superimposed spectra of dansyl-free **2** and of the reference dansyl monomer **1** (Figure 1, a). In particular, the three absorption bands at 218, 252, and 338 nm can be ascribed to the appended dansyl tweezer.

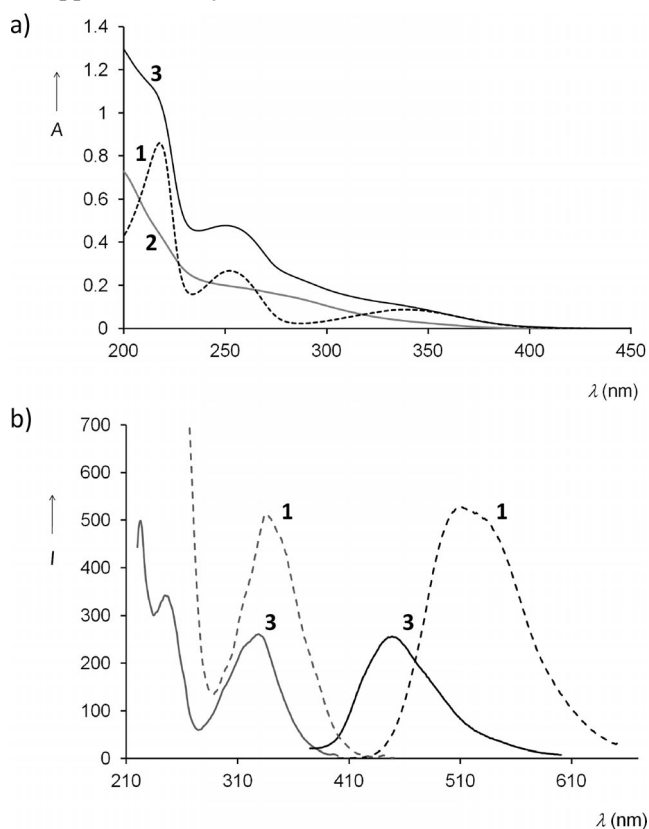


Figure 1. (a) UV/Vis spectra of **1** (20  $\mu\text{M}$ ), **2** (10  $\mu\text{M}$ ), and **3** (10  $\mu\text{M}$ ) in  $\text{CH}_3\text{CN}$ ; (b) fluorescence spectra of **1** [2  $\mu\text{M}$ , dashed lines: excitation ( $\lambda_{\text{em}} = 551$  nm) and emission ( $\lambda_{\text{exc}} = 336$  nm)] and **3** [10  $\mu\text{M}$ , solid lines: excitation ( $\lambda_{\text{em}} = 450$  nm) and emission ( $\lambda_{\text{exc}} = 324$  nm)], in  $\text{CH}_3\text{CN}$ .

The fluorescence spectra of **3** (Figure 1, b) retain the typical pattern expected for the dansyl fluorophore with one emission band centered at 449 nm ( $\lambda_{\text{exc}} = 324$  nm), albeit somewhat blue-shifted and with diminished intensity (20-fold) when compared to the reference emission observed for the singlet  $n,\pi^*$  excited state of **1**, upon excitation at 336 nm.

As verified for the dansyl-free POM **2**, the polyoxotungstate component shows only negligible fluorescence so that the excitation spectrum of **3** ( $\lambda_{\text{em}} = 450$  nm) is dominated by the dansyl contribution, exhibiting well-resolved bands at 223, 245, and 329 nm.

### Protonation Equilibria of Hybrid **3**

Hybrid **3** (10  $\mu\text{M}$ ) undergoes protonation equilibria in acetonitrile/water (97.5:2.5 v/v) upon addition of acid (HCl,  $1.6 \times 10^{-3}$  M). The spectrophotometric titration shows major modifications in the spectral range 210–410 nm, whereby a gradual decrease of the bands at 342 and 250 nm is accompanied by a progressive increase in a new absorption at 293 nm, giving rise to four isosbestic points at 222, 236, 274, and 308 nm (Figure 2, a).

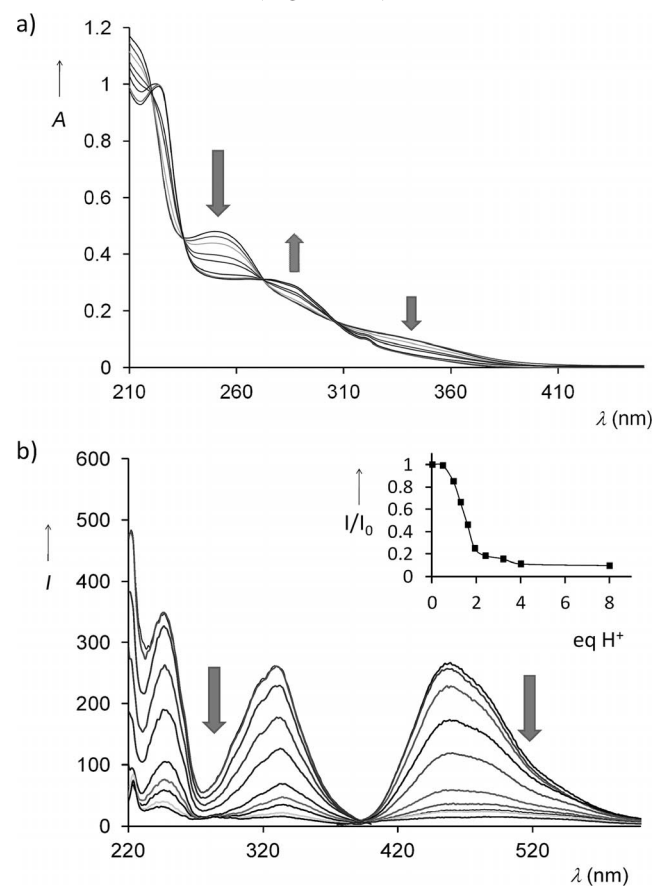


Figure 2. Titration of **3** (10  $\mu\text{M}$  in  $\text{CH}_3\text{CN}$ ) with aqueous HCl ( $1.6 \times 10^{-3}$  M). (a) UV/Vis spectra; (b) Excitation ( $\lambda_{\text{em}} = 450$  nm) and emission ( $\lambda_{\text{exc}} = 324$  nm) spectra. Inset: relative emission intensity at 450 nm upon excitation at 236 nm (one of the isosbestic points).

A parallel modification is registered in the emission and excitation spectra (Figure 2, b), where a progressive decrease of the dansyl-centered bands is observed respectively at 450 ( $\lambda_{\text{exc}} = 324$  nm) and at 247 and 330 nm ( $\lambda_{\text{em}} = 450$  nm). This behavior is consistent with the protonation of both dansyl amino groups, and is responsible for a gradual disappearance of the charge-transfer bands involving the nitrogen lone-pair, as experimentally observed in both the absorption and fluorescence spectra.<sup>[17]</sup>

The protonated H-3 complex can be selectively excited upon irradiation at 293 nm (Figure 2, a), thus promoting emission at 344 and 461 nm (Figure S14–15). During acid titration, the band at 344 nm, ascribed to the naphthalenic emission of H-3, increases, while the longer wavelength band, due to the emission of non-protonated 3, decreases. The spectrophotometric titrations determined either in absorption, emission, or excitation modes, display similar profiles, as a function of the added acid equivalents, and highlight the independent behavior of the dansyl units (Figure 3 and S16).<sup>[17]</sup>

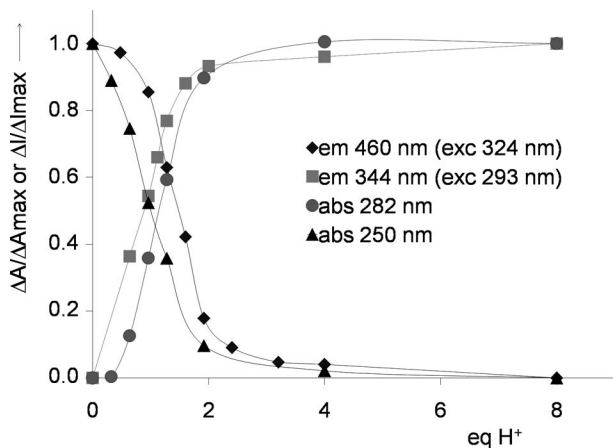


Figure 3. Spectrophotometric titration of 3 (10  $\mu\text{M}$  in  $\text{CH}_3\text{CN}$ ) by stepwise addition of aqueous HCl (1.6  $\mu\text{M}$ ). Normalized values of absorbance (A) and fluorescence intensity (I) variations monitored at different wavelengths.

In all cases, the observed spectral variations can mainly be ascribed to the dansyl probe, and they follow a sigmoidal behavior, with an initial “silent” phase, which was clearly determined in the fluorescence titration, followed by a linear behavior to a plateau value reached at two equivalents. This is likely explained by an initial buffering effect of the inorganic polyanion, which acts as a competing proton scavenger in the system.<sup>[29]</sup>

This hypothesis has been addressed by DFT calculations by using the ZORA-BP86 functional with the TZ2P basis set, including solvent and relativistic effects. Due to the large size of the molecules and to the high number of heavy metals, the internal or core electrons were kept frozen (see Exp. Sect.). These methods provide the optimized geometry for 3, together with the molecular electrostatic potential (MEP), and frontier molecular orbital (FMO) analysis (Figure 4). MEP analysis allowed the relative basicity of the different sites in the molecular hybrid to be estimated and indicated that a significant and extended electron density was localized at the oxygen centers of the polyoxometalate framework (Figure 4, a). Moreover, inspection of the calculated FMO distribution showed that the filled orbitals were delocalized on the oxygen POM centers (oxo band) with energy levels close to the dansyl HOMO and HOMO–1, mostly identified by the  $\pi$  orbitals of the naphthalenic units with approximately 30% contribution of the p orbital of the nitrogen atoms of the dimethylamino functions (Figure 4,

b). These findings support the involvement of the POM scaffold in protonation equilibria.

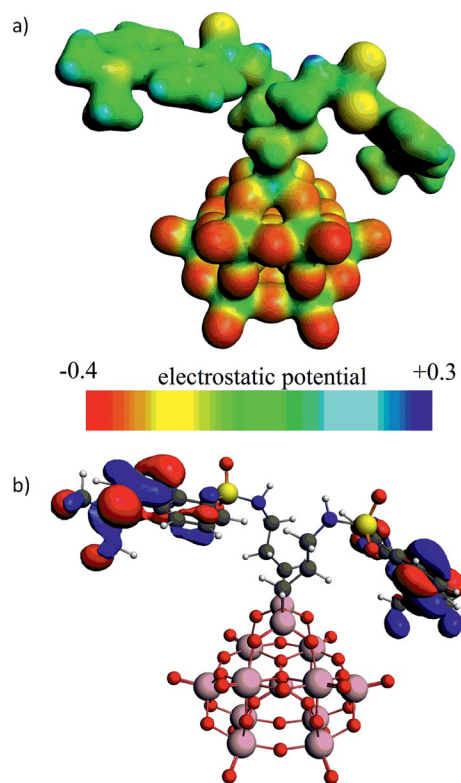


Figure 4. (a) Map of the electrostatic potential and (b) representation of the HOMO and HOMO–1 orbitals of 3, delocalized in the dansyl moieties.

### Fluoroionophore Properties of 3

To evaluate the optical response of hybrid 3 towards other cationic analytes and its potential as a fluorescent chemosensor for metal ions, emission quenching experiments were performed in the presence of  $\text{Cu}^{2+}$ ,  $\text{Fe}^{2+}$ ,  $\text{Ni}^{2+}$ ,  $\text{Hg}^{2+}$ ,  $\text{Co}^{2+}$ ,  $\text{Cd}^{2+}$ ,  $\text{Zn}^{2+}$ , and  $\text{Pb}^{2+}$  by addition of an aqueous analyte solution (1.6 mM) to 3 (10  $\mu\text{M}$  in  $\text{CH}_3\text{CN}$ ). The bar-graph in Figure 5 highlights the dependence of the fluo-

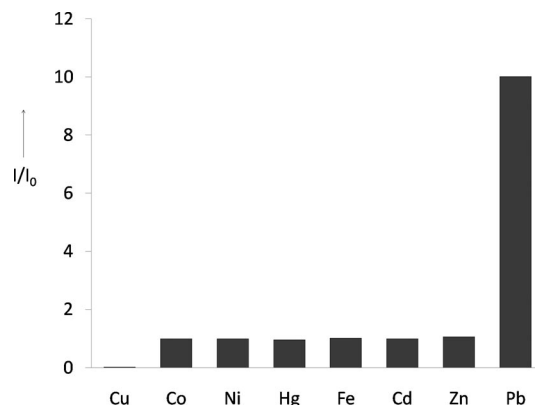


Figure 5. Optical sensing screening determined as the ratio between the fluorescence intensity observed for 3 (10  $\mu\text{M}$  in  $\text{CH}_3\text{CN}$  with 2.5% v/v  $\text{H}_2\text{O}$ ) in the absence of any metal ion ( $I_0$ ) and in the presence of 40  $\mu\text{M}$  metal ions ( $I_M$ ) ( $\lambda_{\text{exc}} = 324$  nm;  $\lambda_{\text{em}} = 457$  nm, for  $\text{Pb}^{2+}$   $\lambda_{\text{em}} = 525$ ).

rescence intensity ratio  $I_M/I_0$  determined at  $\lambda_{em} = 457$  ( $\lambda_{ex} = 324$  nm) as a function of the metal ion added in the system.

In most cases, no appreciable change in the emission intensity occurred ( $I_M/I_0 \approx 1$ ), with the remarkable exceptions of  $\text{Cu}^{2+}$  and  $\text{Pb}^{2+}$ , which are two ions that are typically recognized as hazardous contaminants for drinking water.<sup>[30]</sup> The optical sensing by **3** clearly entails diverse recognition mechanisms, because opposite effects are induced in the fluorescence emission upon addition of either  $\text{Cu}^{2+}$  or  $\text{Pb}^{2+}$  analyte.

In particular, sensing of aqueous  $\text{PbSO}_4$  (40  $\mu\text{M}$ ), was determined by a redshift (68 nm) of the maximum emission wavelength ( $\lambda = 525$  nm), together with a progressive ten-fold increase of luminescence at that wavelength (Figure S17). Fluorescence enhancement has been previously reported for dansyl-based  $\text{Pb}^{2+}$  ionophores, which was ascribed to metal ligation upon deprotonation of the NH amide function.<sup>[25]</sup> In this specific case, however,  $\text{Pb}^{2+}$  ions may trigger a change either in the electronic structure or in the interactions between the chromophoric units, such as a decreased stacking of paired naphthalenic moieties. The similar emission of the  $\text{Pb}^{2+}$  adduct and of derivative **1** may also suggest a reduced interaction between the dansyl units and the polyanionic domain.

On the other hand, stepwise addition of  $\text{CuSO}_4$  ( $1.6 \times 10^{-3}$  M, ca. 4  $\mu\text{L}$  aliquots) induced a progressive quenching of the emission band, monitored at 457 and at 525 nm ( $\lambda_{exc} = 324$  nm), down to a plateau value of about 5–14% with respect to the initial conditions (Figure 6).

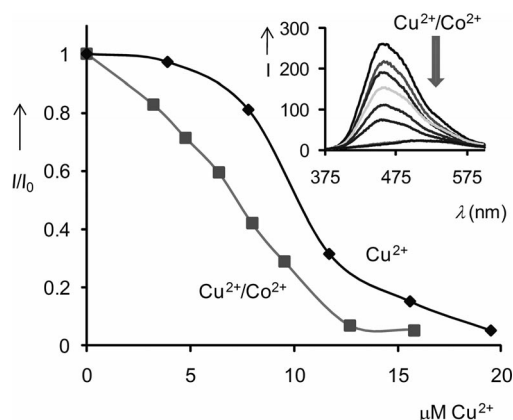


Figure 6. Normalized values of fluorescence intensity ( $I$ ) obtained for the titration of hybrid **3** (10  $\mu\text{M}$  in  $\text{CH}_3\text{CN}$ ) with an aqueous  $\text{CuSO}_4$  solution (0–20  $\mu\text{M}$ ), in the presence and in the absence of 40  $\mu\text{M}$   $\text{CoSO}_4$ .

The  $\text{Cu}^{2+}$  titration profile resembles the protonation curve, determined for **3** with a similar procedure, again showing a sigmoidal shape, with a turning point at about 1:1 equiv. ratio. Moreover, the UV/Vis spectrum registered for **3** in the presence of the cuprous salt retains isosbestic points (albeit with a lower absolute  $\Delta\text{Abs}$ ) similar to those ascribed to the protonation equilibria (Figure S18). Accordingly, a plausible trigger for the  $\text{Cu}^{2+}$ -induced emission quenching could originate from its binding at the electron-rich amine sites of the luminophore moiety.

For comparison, the fluorescence response of monomeric reference **1** was evaluated with respect to  $\text{Cu}^{2+}$ , which showed negligible activity. This observation highlights the interplay between the two domains in the sensing mechanisms. Indeed, at variance with the majority of previously reported Cu-chemosensors, **3** does not contain any additional binding site tailored for a specific transition metal.<sup>[31]</sup> Selective sensing by **3** and the tuning of its optical response stems from its multi-functional molecular nature integrating a dansyl-based optical transducer with a nano-dimensional tungsten-oxide polyanionic surface. This latter feature is instrumental for the geometrical constrains/spacing of the bis-fluorophore tweezer, the shaping of its solvation environment, and the occurrence of competing cation scavenging equilibria that can be exploited in the analysis of complex mixtures. Indeed, the selective recognition of  $\text{Cu}^{2+}$  by **3** has also been validated in the presence of potentially interfering bivalent metal ions such as  $\text{Fe}^{2+}$ ,  $\text{Ni}^{2+}$ ,  $\text{Co}^{2+}$ , and  $\text{Zn}^{2+}$ . The presence of these latter ions did not result in any detrimental effects in the system, even when added in large excess (40  $\mu\text{M}$ ). On the other hand, the combined presence of “dansyl-silent” metal cations, for instance  $\text{Co}^{2+}$ , turns out to improve the optical signaling of  $\text{Cu}^{2+}$ , resulting in a linearization of the sigmoidal fluorescence titration curve (Figure 6). This can be explained by a preferential electrostatic interaction between  $\text{Co}^{2+}$  and the POM surface, thus switching off its masking effect for the competing  $\text{Cu}^{2+}$ , and overriding the initial lag-response of the dansyl fluorophore.<sup>[32]</sup> Under such optimized conditions, a linear correlation is obtained, featuring a micromolar detection limit with maximum quenching at  $[\text{Cu}^{2+}]$  above 12  $\mu\text{M}$ , pointing to a 1:1 interaction with **3**.

### Supramolecular Properties of Hybrid **3** and Thin Film Heterogenization

Because of its composite but well-defined molecular structure, hybrid **3** provides a functional model vis-à-vis the emerging area of nano-supported chemosensors.<sup>[17,33]</sup> The key motif of surface-implemented systems is the organization of fluorophore arrays where spatial proximity is such that multiple electron/energy transfer events are leveraged, thus enhancing optical sensing.<sup>[17]</sup>

Aggregation/surface phenomena can be envisaged for hybrid **3** to take place as a result of its organic–inorganic and amphiphilic nature, which is likely to yield extended supramolecular architectures as a function of the solvent composition. To shed light into the solution structure of **3** (10  $\mu\text{M}$ ) under the sensing conditions, Dynamic Light Scattering (DLS) experiments were performed in  $\text{CH}_3\text{CN}$  with added water (2.5% v/v). In this medium, DLS analysis allowed the characterization of spherical aggregates with average hydrodynamic radius  $R_h = 800$  nm and a broad size distribution (Figure S19); control analysis in neat  $\text{CH}_3\text{CN}$  give no evidence of any supramolecular phenomena.

Scanning electron microscopy (SEM) images confirmed the formation of vesicular structures upon addition of more

than 0.5% water to a  $\text{CH}_3\text{CN}$  solution (Figure 7c). Their size range is consistent with the DLS evidence, displaying an average diameter of approximately  $1\ \mu\text{m}$ .<sup>[34,35]</sup>

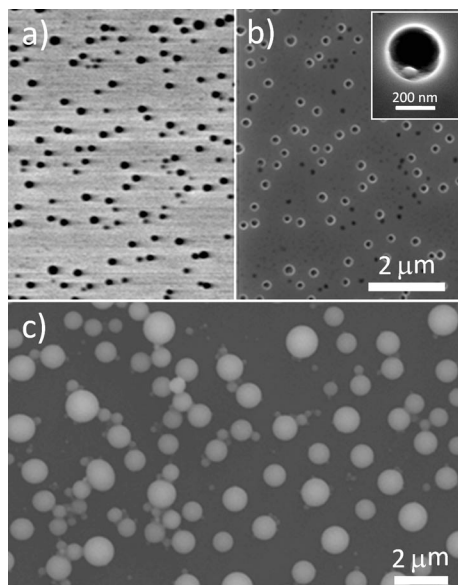


Figure 7. (a) and (b) SEM micrographs of **3**, drop casted from a  $10\ \mu\text{M}$   $\text{CH}_3\text{CN}$  solution [backscattered signal (left image) highlights dark regions, without POMs], and (c) from a  $\text{CH}_3\text{CN}$  solution containing 0.5%  $\text{H}_2\text{O}$ .

Amphiphilic POMs are known to yield well-defined supramolecular architectures, including vesicles, bilayer structures, and nano-objects with different morphology.<sup>[36]</sup> These are mainly hybrid salts that are obtained by a tailored choice of the organic counterion, as in the well-known surfactant encapsulated POMs.<sup>[37]</sup>

In the present system, the molecular unit is engineered to incorporate directional covalent bonds connecting the inorganic scaffold to an organic area with hydrophobic aromatic substituents.<sup>[38]</sup> These latter moieties can drive recognition/association phenomena while also providing the functional site of the system.

A solvent-casting film of **3** deposited on a silicon wafer from a wet acetonitrile solution ( $10\ \mu\text{m}$ ) featured an extended area of POM-containing material (as highlighted by the SEM, acquired with both secondary and backscattered electron signals, Figure 7 a–b) with a surface distribution of nanostructured cavities displaying a  $200\ \text{nm}$  diameter and POM exposed on the inner walls (inset in Figure 7, b).

A porous architecture is instrumental for combining transport/separation properties with sensing/recognition functions, and this is likely ascribed to the templating effect of POM amphiphiles organized as supramolecular vesicles and acting as porogenic sites on solvent evaporation. Such behavior has been previously observed for hybrid POM salts,<sup>[39]</sup> and can be exploited for the tailored fabrication of flat membranes implementing mechanical resistance and selective separation/optical sensing functions.

The covalent strategy used in POM hybrids is therefore expected to ultimately shape innovative multi-component

materials, which hold great promise for applications in organic/inorganic-based molecular devices.<sup>[40]</sup>

To evaluate the potential of **3** as a supramolecular synthon for three dimensional networks and sensing devices, thin film formation was preliminarily addressed by SEM studies after inclusion within polymeric membranes.<sup>[41]</sup>

To this end, vesicle aggregates of **3** were embedded within a hydrophobic fluorinated polymer by blending polyvinylidene difluoride (PVDF) and POM **3** in dimethylacetamide solution (DMA) (16:1:83% w/w). After solvent casting, membrane separation was obtained by phase inversion in an aqueous bath.<sup>[42]</sup> The resulting film ( $300\ \mu\text{m}$  thickness), featured a homogeneous distribution of nanoclusters of **3** (SEM image in Figure 8, a) with average diameter  $90\ \text{nm}$  that were roughly distributed in pillared arrays (Figure 8, b) thus fostering a high surface area and an irregular cross-section. It is noteworthy that the membrane luminescence was maintained upon irradiation with a  $366\text{-nm}$  lamp (Figure S22), emitting blue–green fluorescence. Moreover, fine tuning of the polymer blend vis-à-vis surface properties and wettability is expected to allow the preparation of ON/OFF luminescent devices.<sup>[41]</sup>

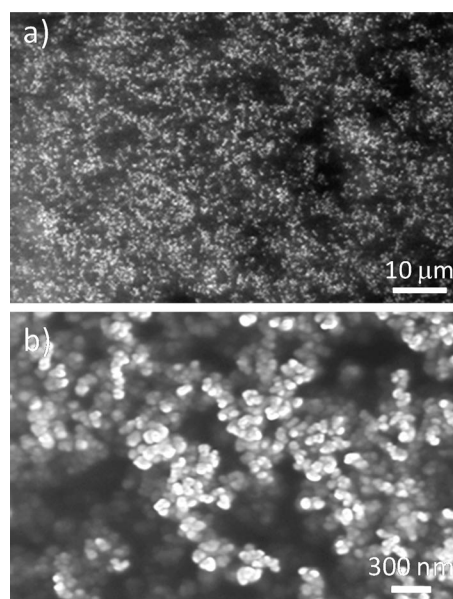


Figure 8. SEM micrographs of **3@PVDF** at different magnifications (top side of the membrane). Bright areas identify the POM-containing material.

## Conclusions

The two-step synthetic procedure reported herein targets the organic–inorganic covalent assembly of innovative polyoxometalate-based molecular chemosensors displaying recognition and luminescent signaling functions. The selective functionalization of the lacunary Keggin-type polyoxotungstate  $[\gamma\text{-SiW}_{10}\text{O}_{36}]^{8-}$ , which provides a highly robust, rigid, and polyanionic nano-scaffold, has been successfully exploited to shape a tweezer-like arrangement of a bis-dansyl-sulfonamide moiety. The resulting hybrid **3** has been char-

acterized in the solid state and in solution by a combination of spectroscopic and electron microscopy techniques to ascertain its covalent bond connectivity, protonation state, optical properties, and supramolecular aggregation state. The formation of vesicles was detected in acetonitrile/aqueous media and was likely driven by the organic/inorganic amphiphilic nature of the POM hybrid. The POM-based bis-dansyl tweezer acts as a selective fluorescence sensor for  $\text{Cu}^{2+}$  and  $\text{Pb}^{2+}$  ions, in quenching and enhancing mode, respectively, with tunable intensity that depends on the emission wavelength, POM-aided scavenging of potentially interfering cations, and a detection limit in the micromolar range. Whereas the reference monomer **1** displays negligible sensing activity, **3** shows some remarkable benefits with respect to previously known nano-colloid analogues: (i)  $\text{Cu}^{2+}$ / $\text{Pb}^{2+}$  sensing is achieved by implementing the luminescent components in the tweezer arrangement, without the need to integrate a tailored multi-dentate fragment; (ii) tuning of the solubility as a function of the POM counterions can be used to exploit typical dansyl-induced solvatochromism; (iii) POM-templated three-dimensional porous architectures in thin films and flexible membranes have potential in optical devices.

Our effort is now directed towards the surface decoration of POM molecules with asymmetric fluorescent dyads exhibiting tailored photophysical properties with the aim of expanding the field of applications.

## Experimental Section

**General:** All reagents were purchased from commercial sources and used as received, without further purification.  $\text{K}_8[\gamma\text{-SiW}_{10}\text{O}_{36}]$  was prepared as described in the literature.<sup>[43]</sup>  $^1\text{H}$  NMR spectra were recorded with Bruker AV300 instruments operating at 300.13 MHz.  $^{13}\text{C}$  NMR spectra were recorded with a Bruker AV300 operating at 75.4 MHz;  $\text{Si}(\text{CH}_3)_4$  was used as reference.  $^{183}\text{W}$  and  $^{29}\text{Si}$  NMR spectra were recorded with a Bruker Avance DRX 400 instrument operating at 16.67 and 79.50 MHz, respectively, using 2 M  $\text{Na}_2\text{WO}_4$  in  $\text{D}_2\text{O}$  and  $\text{Si}(\text{CH}_3)_4$  in  $\text{CDCl}_3$  as external references. FTIR (KBr) spectra were collected with a Thermo Quest Nicolet 5700 instrument. ESI-MS spectra were obtained with a Agilent LC/MSD Trap SL spectrometer, by using a capillary potential of 1500 V. Fluorimetric analyses were performed with a Perkin–Elmer LS50B instrument with 1 cm quartz cell. Dynamic light scattering was performed with a Malvern Zetasizer Nano-S instrument. Field emission scanning electron microscopy (FE-SEM) measurements were carried out at acceleration voltages between 5.0 and 20.0 kV with a Zeiss SUPRA 40VP instrument.

**$(n\text{Bu}_4\text{N})_4[\{(\text{CH}_3)_2\text{N}\}_4\text{C}_{10}\text{H}_6\text{SO}_2\text{NH}(\text{CH}_2)_3\text{Si}\}_2\text{O}(\gamma\text{-SiW}_{10}\text{O}_{36})]$ :** In a round-bottomed flask, **2** (400 mg, 0.12 mmol) was suspended in acetonitrile (3 mL). Triethylamine (58  $\mu\text{L}$ , 0.42 mmol) was slowly added under vigorous stirring. After for 5 min, dansyl chloride (112 mg, 0.415 mmol) was dissolved in acetonitrile (4 mL) and added to the solution whilst stirring. The mixture was heated at 40 °C under reflux for 2.5 h and then centrifuged to remove insoluble reagents and byproducts. The volume of the solution was reduced to 1 mL by evaporation under vacuum, then diethyl ether was added to precipitate the product. The solid was washed with water and diethyl ether on a fritted funnel and dried for several hours under vacuum. Yield: 366 mg (0.09 mmol, 69%).

$\text{C}_{94}\text{H}_{182}\text{N}_8\text{O}_{41}\text{S}_2\text{Si}_3\text{W}_{10}$  (4067.38): calcd. C 27.75, H 4.51, N 2.75, S 1.58; found C 25.87, H 4.45, N 2.82, S 1.06. FTIR (KBr):  $\tilde{\nu}$  = 2961 (m), 2938 (m), 2873 (m), 634 (w,b), 1476 (m), 1394 (w), 1316 (w), 1146 (m), 1102 (m), 1043 (m,b), 967 (m), 906 (s), 885 (s), 821 (s), 792 (s), 741 (s, m), 684 (m), 625 (m), 569 (m), 544 (m), 508 (m)  $\text{cm}^{-1}$ .  $^1\text{H}$  NMR (300 MHz,  $\text{CD}_3\text{CN}$ , 301 K):  $\delta$  = 0.24 (m, 4 H,  $\text{N}(\text{CH}_2\text{CH}_2\text{CH}_2\text{Si})$ ), 0.97 [t,  $^3J$  = 8.7 Hz, 48 H,  $\text{N}(\text{CH}_2\text{CH}_2\text{CH}_2\text{CH}_3)_4$ ], 1.31 [m, 36 H,  $\text{N}(\text{CH}_2\text{CH}_2\text{CH}_2\text{CH}_3)_4$  and  $\text{SiCH}_2\text{CH}_2\text{CH}_2\text{N}$ ], 1.62 [m, 32 H,  $\text{N}(\text{CH}_2\text{CH}_2\text{CH}_2\text{CH}_3)_4$ ], 2.84 [m, 16 H,  $\text{N}(\text{CH}_3)_2$  and  $\text{SiCH}_2\text{CH}_2\text{CH}_2\text{N}$ ], 3.14 [m, 32 H,  $\text{N}(\text{CH}_2\text{CH}_2\text{CH}_2\text{CH}_3)_4$ ], 5.95 (t,  $^3J$  = 6.0 Hz, 2 H,  $\text{NHCH}_2\text{CH}_2\text{CH}_2\text{Si}$ ), 7.22 (m, 2 H, Ar-H), 7.58 (m, 4 H, Ar-H), 8.16 (m, 2 H, Ar-H), 8.30 (d,  $^3J$  = 8.7 Hz, 2 H, Ar-H), 8.48 (d,  $^3J$  = 8.4 Hz, 2 H, Ar-H) ppm.  $^{13}\text{C}\{^1\text{H}\}$  NMR (75.47 MHz,  $\text{CD}_3\text{CN}$ , 301 K):  $\delta$  = 13.01 (2 C,  $\text{SiCH}_2\text{CH}_2\text{CH}_2\text{N}$ ), 14.07 [16 C,  $\text{N}(\text{CH}_2\text{CH}_2\text{CH}_2\text{CH}_3)_4$ ], 20.47 [16 C,  $\text{N}(\text{CH}_2\text{CH}_2\text{CH}_2\text{CH}_3)_4$ ], 24.51 [16 C,  $\text{N}(\text{CH}_2\text{CH}_2\text{CH}_2\text{CH}_3)_4$ ], 24.73 (2 C,  $\text{SiCH}_2\text{CH}_2\text{CH}_2\text{N}$ ), 45.83 [4 C,  $\text{N}(\text{CH}_3)_2$ ], 46.83 (2 C,  $\text{SiCH}_2\text{CH}_2\text{CH}_2\text{N}$ ), 59.40 [16 C,  $\text{N}(\text{CH}_2\text{CH}_2\text{CH}_2\text{CH}_3)_4$ ], 124.53, 129.27, 129.99, 130.50, 130.70, 136.82, 152.87 (20 C, Ar) ppm.  $^{183}\text{W}$  NMR (16.67 MHz,  $\text{CD}_3\text{CN}/\text{CH}_3\text{CN}$ , 298 K):  $\delta$  = -107.9 (4 W), -136.2 (2 W), -142.1 (4 W) ppm.  $^{29}\text{Si}$  NMR (79.49 MHz,  $\text{CD}_3\text{CN}/\text{CH}_3\text{CN}$ , 298 K):  $\delta$  = -62.5 (2 Si), -88.4 (1 Si) ppm. ESI-MS (-ve,  $\text{CH}_3\text{CN}$ ): calcd. for  $[\text{C}_{30}\text{H}_{36}\text{N}_4\text{O}_{41}\text{S}_2\text{Si}_3\text{W}_{10}]^{4-}$  773.3; found 773.9. UV:  $\lambda$  (log  $\epsilon$ ) = 251 (4.7), 211 (5.1) nm.

**Fluorimetric Titrations:**  $\text{CuSO}_4 \cdot 5\text{H}_2\text{O}$ ,  $\text{Zn}(\text{NO}_3)_2 \cdot 6\text{H}_2\text{O}$ ,  $\text{HgSO}_4$ ,  $\text{PbSO}_4$ ,  $\text{NiSO}_4 \cdot 6\text{H}_2\text{O}$ ,  $\text{FeSO}_4$ ,  $\text{CdSO}_4 \cdot \text{H}_2\text{O}$ , and  $\text{CoSO}_4 \cdot 6\text{H}_2\text{O}$  were analytical-grade products and were used to prepare 1.6 mM aqueous solutions. 2 mL of a 10  $\mu\text{M}$   $\text{CH}_3\text{CN}$  solution of **3** were placed in a fluorescence quartz cell. A variable volume of concentrated metal ion solution (up to 40  $\mu\text{L}$ ) was added, and water was added to provide a fixed 2.5% water content. The resulting solutions were allowed to equilibrate until stable emission spectra were obtained (less than 5 min were usually required, except for  $\text{Pb}^{2+}$ ).

**Membrane Preparation:** In a vial, **3** (20 mg), PVDF (300 mg), and dimethylacetamide (1.6 g) were stirred overnight. The viscous mixture was cast on a glass surface using a casting knife set at 300  $\mu\text{m}$ . The mixture was then immersed in water until the membrane, formed by phase inversion, separated from the glass surface. The film was thoroughly washed with water, dried under vacuum at 65 °C for 2 h and then placed in an oven at 65 °C for 12 h.

**DFT Calculations:** Computational resources and assistance were provided by the Laboratorio Interdipartimentale di Chimica Computazionale (LICC) at the Department of Chemical Sciences of the University of Padova. DFT calculations were carried out using the Amsterdam density functional (ADF) code,<sup>[44]</sup> scalar relativistic effects were taken into account by means of the two-component zero-order regular approximation (ZORA) method,<sup>[45]</sup> adopting the Becke 88 exchange plus the Perdew 86 correlation (BP) functional.<sup>[46]</sup> The basis functions for describing the valence electrons are triple-zeta quality, doubly polarized (TZ2P), specially optimized for ZORA calculations. Due to the large size of the molecules under investigation, the internal or core electrons (C, N and O: 1s; Si: 1s to 2sp; W: 1s to 4spdf) were kept frozen. Geometries were optimized without symmetry constraints. The solvent effect was modeled by means of the ADF implementation<sup>[47]</sup> of the COSMO method.<sup>[48]</sup>

**Supporting Information** (see footnote on the first page of this article): Synthesis and characterization of compounds **1** and **2**, spectra not reported in the paper, other SEM images, selectivity test by fluorimetric analysis, optimized geometry coordinates.

## Acknowledgments

Financial support from the University of Padova (PRAT CPDA084893/08), Progetto Strategico 2008 HELIOS (STPD08RCX), Ministero dell'Università e della Ricerca (MIUR) (PRIN contract number 20085M27SS and FIRB code RBAP11-ETKA\_006) and Fondazione Cariparo (Nano-Mode, progetti di eccellenza 2010) are gratefully acknowledged. We thank Antonio Sorarù for DLS analysis.

- [1] a) *Polyoxometalate Chemistry from Topology via Self-Assembly to Applications* (Eds.: M. T. Pope, A. Müller), Kluwer Academic Publishers, Dordrecht, The Netherlands, **2001**; b) *Polyoxometalate Molecular Science* (Eds.: J. J. Borrás-Almenar, E. Coronado, A. Müller, M. T. Pope), Kluwer Academic Publishers, Dordrecht, The Netherlands, **2003**; c) D. L. Long, E. Burkholder, L. Cronin, *Chem. Soc. Rev.* **2007**, *36*, 105–121.
- [2] a) M. Carraro, M. Carraro, G. Scorrano, U. Kortz, *Adv. Synth. Catal.* **2005**, *347*, 1909–1912; b) M. Bonchio, M. Carraro, A. Farinazzo, A. Sartorel, G. Scorrano, U. Kortz, *J. Mol. Catal. A* **2007**, *262*, 36–40; c) A. Sartorel, M. Carraro, R. De Zorzi, S. Geremia, N. D. McDaniel, S. Bernhard, G. Scorrano, M. Bonchio, *J. Am. Chem. Soc.* **2008**, *130*, 5006–5007.
- [3] a) D. A. Judd, J. H. Nettles, N. Nevins, J. P. Snyder, D. C. Liotta, J. Tang, J. Ermolieff, R. F. Schinazi, C. L. Hill, *J. Am. Chem. Soc.* **2001**, *123*, 886–897; b) S. Shigetani, S. Mori, E. Kodama, J. Kodama, K. Takahashi, T. Yamase, *AntiViral Res.* **2003**, *58*, 265–271; c) X. Wang, J. Liu, M. T. Pope, *Dalton Trans.* **2003**, 957–960; d) B. Hasenknopf, *Front. Biosci.* **2005**, *10*, 275–287; e) J. Geng, M. Li, J. Ren, E. Wang, X. Qu, *Angew. Chem. Int. Ed.* **2011**, *50*, 4184–4188; f) G. Geisberger, S. Paulus, M. Carraro, M. Bonchio, G. R. Patzke, *Chem. Eur. J.* **2011**, *17*, 4619–4625.
- [4] a) A. Proust, R. Thouvenot, P. Gouzerh, *Chem. Commun.* **2008**, 1837–1852; b) W. Qi, L. Wu, *Polym. Int.* **2009**, *58*, 1217–1225.
- [5] a) P. Gouzerh, A. Proust, *Chem. Rev.* **1998**, *98*, 77–112; b) A. Dolbecq, E. Dumas, C. R. Mayer, P. Mialane, *Chem. Rev.* **2010**, *110*, 6009–6048; c) S. Berardi, M. Carraro, A. Sartorel, G. Modugno, M. Bonchio, *Isr. J. Chem.* **2011**, *51*, 259–274; d) S. Thorimbert, B. Hasenknopf, E. Lacôte, *Isr. J. Chem.* **2011**, *51*, 275–280.
- [6] a) M. Carraro, L. Sandei, A. Sartorel, G. Scorrano, M. Bonchio, *Org. Lett.* **2006**, *8*, 3671–3674; b) S. Berardi, M. Bonchio, M. Carraro, V. Conte, A. Sartorel, G. Scorrano, *J. Org. Chem.* **2007**, *72*, 8954–8957.
- [7] a) F. M. Toma, A. Sartorel, M. Iurlo, M. Carraro, P. Parisse, C. Maccato, S. Rapino, B. Rodriguez Gonzalez, H. Amenitsch, T. Da Ros, L. Casalis, A. Goldoni, M. Marcaccio, G. Scorrano, G. Scoles, F. Paolucci, M. Prato, M. Bonchio, *Nature Chem.* **2010**, *2*, 826–831; b) F. M. Toma, A. Sartorel, M. Iurlo, M. Carraro, S. Rapino, L. Hooper-Burkhardt, T. Da Ros, M. Marcaccio, G. Scorrano, F. Paolucci, M. Bonchio, M. Prato, *ChemSusChem* **2011**, *4*, 1447–1451.
- [8] a) M. Carraro, M. Gardan, G. Scorrano, E. Drioli, E. Fontananova, M. Bonchio, *Chem. Commun.* **2006**, 4533–4535; b) M. Bonchio, M. Carraro, G. Scorrano, E. Fontananova, E. Drioli, *Adv. Synth. Catal.* **2003**, *345*, 1119–1126.
- [9] a) I. Bar-Nahum, R. Neumann, *Chem. Commun.* **2003**, 2690–2691; b) M. De Bruyn, R. Neumann, *Adv. Synth. Catal.* **2007**, *349*, 1624–1628; c) S. Berardi, M. Carraro, M. Iglesias, A. Sartorel, G. Scorrano, M. Albrecht, M. Bonchio, *Chem. Eur. J.* **2010**, *16*, 10662–10666.
- [10] a) D. L. Long, E. Burkholder, L. Cronin, *Chem. Soc. Rev.* **2007**, *36*, 105–121; b) M. Carraro, A. Sartorel, G. Scorrano, C. Maccato, M. H. Dickman, U. Kortz, M. Bonchio, *Angew. Chem.* **2008**, *120*, 7385; *Angew. Chem. Int. Ed.* **2008**, *47*, 7275–7279; c) D.-L. Long, R. Tsunashima, L. Cronin, *Angew. Chem.* **2010**, *122*, 1780; *Angew. Chem. Int. Ed.* **2010**, *49*, 1736–1758.
- [11] a) M. Bonchio, M. Carraro, A. Bagno, G. Scorrano, *Adv. Synth. Catal.* **2004**, *346*, 648–654; b) C. Allain, S. Favette, L.-M. Chamoreau, J. Vaissermann, L. Ruhlmann, B. Hasenknopf, *Eur. J. Inorg. Chem.* **2008**, 3433–3441; c) F. Odobel, M. Séverac, Y. Pellegrin, E. Blart, C. Fosse, C. Cannizzo, C. R. Mayer, K. J. Elliott, A. Harriman, *Chem. Eur. J.* **2009**, *15*, 3130–3138; d) K. J. Elliott, A. Harriman, L. Le Pleux, Y. Pellegrin, E. Blart, C. R. Mayer, F. Odobel, *Phys. Chem. Chem. Phys.* **2009**, *11*, 8767–8773; e) B. Matt, S. Renaudineau, L.-M. Chamoreau, C. Afonso, G. Izzet, A. Proust, *J. Org. Chem.* **2011**, *76*, 3107–3112; f) B. Matt, C. Coudret, C. Viala, D. Jouvenot, F. Loiseau, G. Izzet, A. Proust, *Inorg. Chem.* **2011**, *50*, 7761–7768.
- [12] a) F. Puntoriero, G. La Ganga, A. Sartorel, M. Carraro, G. Scorrano, M. Bonchio, S. Campagna, *Chem. Commun.* **2010**, 46, 4725–4727; b) M. Orlandi, R. Argazzi, A. Sartorel, M. Carraro, G. Scorrano, M. Bonchio, F. Scandola, *Chem. Commun.* **2010**, 46, 3152–3154.
- [13] a) S. Bareyt, S. Piligkos, B. Hasenknopf, P. Gouzerh, E. Lacôte, S. Thorimbert, M. Malacria, *J. Am. Chem. Soc.* **2005**, *127*, 6788–6794; b) K. Micoine, B. Hasenknopf, S. Thorimbert, E. Lacôte, M. Malacria, *Angew. Chem.* **2009**, *121*, 3518; *Angew. Chem. Int. Ed.* **2009**, *48*, 3466–3468; c) M. Carraro, G. Modugno, A. Sartorel, G. Scorrano, M. Bonchio, *Eur. J. Inorg. Chem.* **2009**, 5164–5174.
- [14] a) C. Minelli, S. B. Lowe, M. M. Stevens, *Small* **2010**, *6*, 2336–2357; b) J. Xie, S. Lee, X. Chen, *Adv. Drug Delivery Rev.* **2010**, *62*, 1064–1079.
- [15] a) L. Zheng, Z. J. Gu, Y. Ma, G. J. Zhang, J. N. Yao, B. Keita, L. Nadjo, *J. Biol. Inorg. Chem.* **2010**, *15*, 1079–1085; b) L. Zheng, Y. Ma, G. Zhang, J. Yao, B. Keita, L. Nadjo, *Phys. Chem. Chem. Phys.* **2010**, *12*, 1299–130; c) C. Boglio, G. Lenoble, C. Duhayon, B. Hasenknopf, R. Thouvenot, C. Zhang, R. C. Howell, B. P. Burton-Pye, L. C. Francesconi, E. Lacôte, S. Thorimbert, M. Malacria, C. Afonso, J.-C. Tabet, *Inorg. Chem.* **2006**, *45*, 1389–1398, and references therein.
- [16] a) P. Ceroni, I. Laghi, M. Maestri, V. Balzani, S. Gestermann, M. Gorka, F. Vogtle, *New J. Chem.* **2002**, *26*, 66–75; b) Y. Zheng, J. Orbulescu, X. Ji, F. M. Andreopoulos, S. M. Pham, R. M. Leblanc, *J. Am. Chem. Soc.* **2003**, *125*, 2680–2686; c) J. R. Lakowicz, in: *Principles of Fluorescence Spectroscopy*, Kluwer Academic/Plenum Publishers, New York, 3rd ed., **2006**.
- [17] a) M. Montalti, L. Prodi, N. Zaccheroni, G. Falini, *J. Am. Chem. Soc.* **2002**, *124*, 13540–13546; b) F. Vögtle, S. Gestermann, C. Kauffmann, P. Ceroni, V. Vicinelli, L. De Cola, V. Balzani, *J. Am. Chem. Soc.* **1999**, *121*, 12161–12166.
- [18] N. Wanichacheva, S. Watpathomsub, V. S. Lee, K. Grudpan, *Molecules* **2010**, *15*, 1798–1810.
- [19] a) R. Métivier, I. Leray, B. Lebeau, B. Valeur, *J. Mater. Chem.* **2005**, *15*, 2965–2973; b) T. Gruber, C. Fischer, M. Felsmann, W. Seichter, E. Weber, *Org. Biomol. Chem.* **2009**, *7*, 4904–4917.
- [20] M. Xu, S. Wu, F. Zeng, C. Yu, *Langmuir* **2010**, *26*, 4529–4534.
- [21] E. D. Roper, V. S. Talanov, M. G. Gorbunova, R. A. Bartsch, G. G. Talanova, *Anal. Chem.* **2007**, *79*, 1983–1989.
- [22] a) M. Montalti, L. Prodi, N. Zaccheroni, G. Battistini, S. Marcuz, F. Mancin, E. Rampazzo, U. Tonellato, *Langmuir* **2006**, *22*, 5877–5881.
- [23] R. Métivier, I. Leray, B. Valeur, *Chem. Commun.* **2003**, 996–997.
- [24] S. Pandey, A. Azam, S. Pandey, H. M. Chawla, *Org. Biomol. Chem.* **2009**, *7*, 269–279.
- [25] K. Kaur, S. Kumar, *Dalton Trans.* **2011**, *40*, 2451–2458.
- [26] P. Passaniti, M. Maestri, P. Ceroni, G. Bergamini, F. Vögtle, H. Fakharnabavi, O. Lukin, *Photochem. Photobiol. Sci.* **2007**, *6*, 471–479.
- [27] C. R. Mayer, I. Fournier, R. Thouvenot, *Chem. Eur. J.* **2000**, *6*, 105–110.
- [28] E. Rampazzo, E. Brasola, S. Marcuz, F. Mancin, P. Tecilla, U. Tonellato, *J. Mater. Chem.* **2005**, *15*, 2687–2696.

- [29] A. Sartorel, M. Carraro, A. Bagno, G. Scorrano, M. Bonchio, *Angew. Chem.* **2007**, *119*, 3319; *Angew. Chem. Int. Ed.* **2007**, *46*, 3255–3258.
- [30] a) World Health Organization (WHO), Guidelines for drinking-water quality, Geneva, 2nd ed., **1996**; b) L. Järup, *Br. Med. Bull.* **2003**, *68*, 167–182; c) D. L. Sparks, B. G. Schreurs, *Proc. Natl. Acad. Sci. USA* **2003**, *100*, 11065–11069.
- [31] a) R. Krämer, *Angew. Chem.* **1998**, *110*, 804; *Angew. Chem. Int. Ed.* **1998**, *37*, 772–773; b) A. Torrado, G. K. Walkup, B. Imperiali, *J. Am. Chem. Soc.* **1998**, *120*, 609–610; c) M. Beltramello, M. Gatos, F. Mancin, P. Tecilla, U. Tonellato, *Tetrahedron Lett.* **2001**, *42*, 9143–9146; d) Y. J. Zheng, K. M. Gattás-Asfura, V. Konka, R. M. Leblanc, *Chem. Commun.* **2002**, 2350–2351; e) R. Méallet-Renault, R. Pansu, S. Amigoni-Gerbier, C. Larpent, *Chem. Commun.* **2004**, 2344–2345.
- [32] K. Micoine, B. Hasenknopf, S. Thorimbert, E. Lacôte, M. Malacria, *Org. Lett.* **2007**, *9*, 3981–3984.
- [33] a) E. Brasola, F. Mancin, E. Rampazzo, P. Tecilla, U. Tonellato, *Chem. Commun.* **2003**, 3026–3027; b) M. Arduini, S. Marcuz, M. Montolli, E. Rampazzo, F. Mancin, S. Gross, L. Arme-lao, P. Tecilla, U. Tonellato, *Langmuir* **2005**, *21*, 9314–9321.
- [34] Larger aggregates, with diameters of 3.5  $\mu\text{m}$ , could also be observed, see Figure S21.
- [35] H. Li, H. Sun, W. Qi, M. Xu, L. Wu, *Angew. Chem.* **2007**, *119*, 1322; *Angew. Chem. Int. Ed.* **2007**, *46*, 1300–1303.
- [36] a) T. Zhang, J. Brown, R. J. Oakley, C. F. J. Faul, *Curr. Opin. Colloid Interface Sci.* **2009**, *14*, 62–70; b) A. Nisar, J. Zhuang, X. Wang, *Chem. Mater.* **2009**, *21*, 3745–3751; c) S. Landsmann, C. Lizandara-Pueyo, S. Polarz, *J. Am. Chem. Soc.* **2010**, *132*, 5315–5321; d) A. Nisar, Y. Lu, X. Wang, *Chem. Mater.* **2010**, *22*, 3511–3518; e) A. Nisar, Y. Lu, J. Zhuang, X. Wang, *Angew. Chem.* **2011**, *123*, 3245–3250; *Angew. Chem. Int. Ed.* **2011**, *50*, 3187–3192; f) J. Zhang, Y.-F. Song, L. Cronin, T. Liu, *J. Am. Chem. Soc.* **2008**, *130*, 14408–14409.
- [37] a) W. Bu, H. Li, W. Li, L. Wu, C. Zhai, Y. Wu, *J. Phys. Chem. B* **2004**, *108*, 12776–12782; b) Y. Wang, W. Li, L. Wu, *Langmuir* **2009**, *25*, 13194–13200.
- [38] a) H. Wang, Y. Yan, B. Li, L. Bi, L. Wu, *Chem. Eur. J.* **2011**, *17*, 4273–4282; b) M. H. Rosnes, C. Musumeci, C. P. Pradeep, J. S. Mathieson, D.-L. Long, Y.-F. Song, B. Pignataro, R. Cogdell, L. Cronin, *J. Am. Chem. Soc.* **2010**, *132*, 15490–15492.
- [39] W. Bu, H. Li, H. Sun, S. Yin, L. Wu, *J. Am. Chem. Soc.* **2005**, *127*, 8016–8017.
- [40] a) L. Basabe-Desmonts, J. Beld, R. S. Zimmerman, J. Hernandez, P. Mela, M. F. García Parajó, N. F. van Hulst, A. van den Berg, D. N. Reinhoudt, M. Crego-Calama, *J. Am. Chem. Soc.* **2004**, *126*, 7293–7299; b) L. Ding, X. Cui, Y. Han, F. Lü, Y. Fang, *J. Photochem. Photobiol. A: Chem.* **2007**, *186*, 143–150; c) F. Rambaud, K. Vallé, S. Thibaud, B. Julián-López, C. Sanchez, *Adv. Funct. Mater.* **2009**, *19*, 2896–2905; d) L. P. Ding, Y. Fang, *Chem. Soc. Rev.* **2010**, *39*, 4258–4273.
- [41] a) Y. Zhang, K. M. Gattás-Asfura, C. Li, F. M. Andreopoulos, S. M. Pham, R. M. Leblanc, *J. Phys. Chem. B* **2003**, *107*, 483–488; b) Y. Zheng, J. Orbulescu, X. Ji, F. M. Andreopoulos, S. M. Pham, R. M. Leblanc, *J. Am. Chem. Soc.* **2003**, *125*, 2680–2686.
- [42] M. Mulder, *Basic Principles of Membrane Technology*, 2nd ed., Kluwer Academic Publishers, Dordrecht, The Netherlands, **1996**, pp. 71–156.
- [43] J. Canny, A. Tézé, R. Thouvenot, G. Hervé, *Inorg. Chem.* **1986**, *25*, 2114–2119.
- [44] G. te Velde, F. M. Bickelhaupt, E. J. Baerends, C. Fonseca Guerra, S. J. A. van Gisbergen, J. G. Snijders, T. Ziegler, *J. Comput. Chem.* **2001**, *22*, 931–967.
- [45] a) J. Autschbach, in: *Calculation of NMR and EPR Parameters: Theory and Applications* (Eds.: M. Kaupp, M. Bühl, V. G. Malkin), Wiley-VCH, Weinheim, Germany, **2004**, Chapter 14; b) E. van Lenthe, E. J. Baerends, J. G. Snijders, *J. Chem. Phys.* **1993**, *99*, 4597–4610; c) E. van Lenthe, *Ph. D. Thesis*, Vrije Universiteit, Amsterdam, The Netherlands, **1996**; d) S. K. Wolff, T. Ziegler, E. van Lenthe, E. J. Baerends, *J. Chem. Phys.* **1999**, *110*, 7689–7698.
- [46] a) J. P. Perdew, *Phys. Rev. B* **1986**, *33*, 8822–8824; b) A. D. Becke, *Phys. Rev. A* **1988**, *38*, 3098–3100.
- [47] C. C. Pye, T. Ziegler, *Theor. Chem. Acc.* **1999**, *101*, 396–408.
- [48] a) A. Klamt, G. Schürmann, *J. Chem. Soc. Perkin Trans. 2* **1993**, 799–805; b) A. Klamt, V. Jones, *J. Chem. Phys.* **1996**, *105*, 9972–9981; c) A. Klamt, *J. Phys. Chem.* **1995**, *99*, 2224–2235.

Received: July 30, 2011

Published Online: November 24, 2011